*Materials Transactions*, Vol. 42, No. 12 (2001) pp. 2480 to 2486
Special Issue on Recycling and High Performance Waste Processing


# Phase Relation and Thermodynamic Properties of $NaCl–Na_2CO_3$ System as a Basic System for Secondary Fly Ash in Incineration Processes of Municipal Wastes

Kokoro Iwasawa[1, *], Shu Yamaguchi[2] and Masafumi Maeda[1]

[1]*Institute of Industrial Science, The University of Tokyo, Tokyo 153-8505, Japan*
[2]*Department of Material Science and Engineering, School of Engineering, The University of Tokyo, (Department of Material Science and Engineering, Nagoya Institute of Technology) Tokyo 113-8656, Japan*

The thermodynamic properties and phase relation of an alkali metal-oxychloride system were examined; this is a basic model system of secondary fly ash generated in the volume reduction process of bottom ash and fly ash from incineration processes. The phase diagram for the $NaCl–Na_2CO_3$ system and its thermodynamic properties have been examined by a hot filament method and electromotive force (EMF) method using Na $\beta$-$Al_2O_3$ as a solid electrolyte from 500°C to 900°C. The liquidus lines and the eutectic temperature show good agreement with previous reports. Activities of $Na_2CO_3$ for the $NaCl–Na_2CO_3$ system obtained in this study are compared with the data from the phase diagram.

(Received July 13, 2001; Accepted October 24, 2001)

***Keywords***: *secondary fly ash, hot-filament method, electromotive force (EMF) method, oxychloride system, $NaCl–Na_2CO_3$ system*

## 1. Introduction

Most municipal wastes in Japan are incinerated and gas, bottom ash and fly ash are evolved and processed. Since both bottom ash and fly ash are low in density, the volume must be reduced by a certain treatment at reasonable cost. These two types of ash are mixed and melted, but in turn, the volume reduction process generates a so-called secondary fly ash which contains heavy metals and chlorides.

Fly ash contains solid particles carried by gas and various metallic compounds vaporized and condensed in dust chambers. The basic elements contained in the secondary fly ash are alkali metals, heavy metals, silicon, aluminum, calcium, chlorine, carbon and oxygen. The physical and chemical properties of these mixed and complex compounds, which are termed oxychlorides, are fundamental not only in the treatment of secondary fly ash but also in the processing of various other kinds of solid waste. Since the secondary fly ash is commonly composed of "artificial compounds" which are rarely found in the natural environment, very few studies have been made on the oxychloride systems.

The objective of this work is to clarify the thermodynamic nature of waste-originated oxychlorides in order to develop a novel processing for the conversion of these materials into nonpoisonous stocks and to efficiently recover resources. Among the complex components in the secondary ashes, the $NaCl–Na_2CO_3$ quasi binary system is chosen as a basic model system, because the sodium oxychlorides easily react with $CO_2$ in the atmosphere to form $NaCl–Na_2CO_3$ salt at around operating temperatures. The thermodynamic properties of the sodium–carbon–chlorine–oxygen system have been studied by both hot-filament method and electromotive force (EMF) method.

## 2. Experimental

### 2.1 Measurement of the liquidus and eutectic point of the $NaCl–Na_2CO_3$ system

A schematic illustration of the apparatus used in the hot filament technique is shown in Fig. 1. B-type thermocouples were used ($\phi$0.5 mm Pt–6%Rh/Pt–30%Rh) to hold the sample, in addition to the temperature measurement.[1–4] After a mixture of NaCl and $Na_2CO_3$ was placed on the filament, the temperatures at which the sample state changes, were measured by observing the phase change using an optical microscope. The thermocouple was calibrated by measuring known melting points of the pure substances $Na_2SO_4$, KBr, NaCl and $KNO_3$. A mixture of raw materials weighed to a proper com-

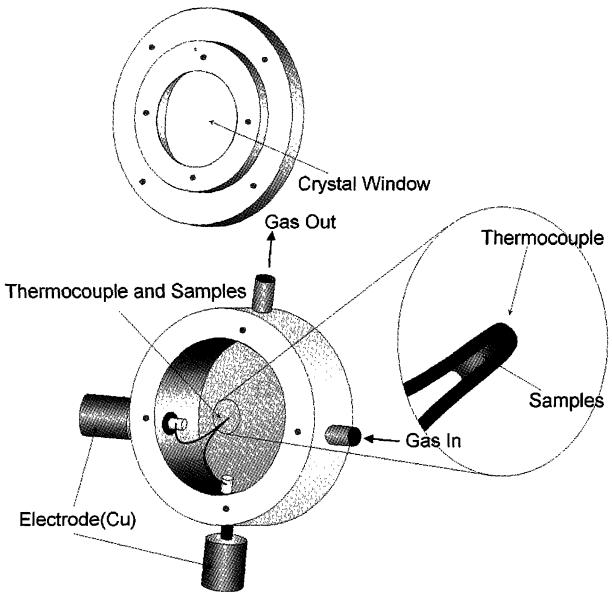


Fig. 1 Schematic illustration of the cell used in the hot filament method.

*Graduate Student, The University of Tokyo.

position was well mixed by a mortar and pestle, and installed in the apparatus. After the premelting treatment on the filament, the sample was subjected to the measurement. The heating and cooling rates were about 30–60°C/min. The cell chamber was maintained in an inert atmosphere by flowing pure argon gas at the flow rate of $5.0 \times 10^{-5}$ m$^3$/min to eliminate water vapor.

### 2.2 Activity measurement of the NaCl–$Na_2CO_3$ system using an EMF method

A concentration-type galvanic cell composed of Na $\beta$-$Al_2O_3$ as a solid state electrolyte was employed to measure the activity of $Na_2CO_3$ in the melts. Previous reports have demonstrated that the transference number of $Na^+$ ions in Na $\beta$-$Al_2O_3$ is essentially unity.[5–7] Many investigators have taken advantage of this property to measure activities of sodium in metallic alloys and the activity of $Na_2O$ in oxide systems.[8–10]

The construction of the galvanic cell can be written as follows:

$$\text{I}\quad \begin{matrix}\text{Au}(s),\ \text{O}_2\text{–CO}_2(g,\ p_{O_2},\ p_{CO_2}) \\ \text{NaCl–Na}_2\text{CO}_3(l,\ s)\end{matrix} \quad\Big|\quad \text{Na}^+ \quad\Big|\quad \begin{matrix}\text{O}_2\text{–CO}_2(g,\ p_{O_2},\ p_{CO_2}),\ \text{Au}(s) \\ \text{Na}_2\text{CO}_3(s)\end{matrix} \quad \text{II}$$

$$\beta - \text{Al}_2\text{O}_3$$

The cathode and anode half-cell reactions are written respectively as follows:

$$2\text{Na}^+ + \frac{1}{2}\text{O}_2 + \text{CO}_2 + e^- = (\text{Na}_2\text{CO}_3)_{\text{NaCl–Na}_2\text{CO}_3} \quad (1)$$

$$(\text{Na}_2\text{CO}_3)_{\text{Na}_2\text{CO}_3(s)} = 2\text{Na}^+ + \frac{1}{2}\text{O}_2 + \text{CO}_2 + 2e^- \quad (2)$$

EMF of the cell can be expressed by the following Nernst's equation,

$$E = \frac{RT}{2F} \ln a_{\text{Na}_2\text{CO}_3} \quad (3)$$

where $E$ is the reversible potential of the cell, $F$ is Faraday's constant and $a_{\text{Na}_2\text{CO}_3}$ is the activity of $Na_2CO_3$. The raoultian standard state is used in this article, where pure solid and liquid $Na_2CO_3$ is used as a standard state below and above the melting temperature.

Reagent grade sodium carbonate and sodium chloride are used as starting materials, after drying treatment at 130°C for 24 h and 750°C for 24 h, respectively. The sample composition is expressed by a nominal one, which is calculated from the weight of $Na_2CO_3$ and NaCl. The EMF measurements were made on samples of $X_{\text{Na}_2\text{CO}_3} = 0.2$, 0.4, 0.5 and 0.7.

A schematic illustration of the electrochemical cell is shown in Fig. 2. The Na $\beta$-$Al_2O_3$ closed one-end tubes used in the present study are produced by Toshiba Ceramics Co., Ltd. and Polyceram (Montreal, Canada). Although part of the electrodes was set in the hot zone kept within ±1°C, the temperature at the top most position of the electrolyte was 10°C lower than that in the electrode position. The hot junction of the R-type thermocouple to measure the cell temperature is placed in contact with the bottom of an alumina crucible which holds the reference $Na_2CO_3$.

A gas mixture of $CO_2$, $O_2$ and Ar is introduced into the cell at an overall flow rate of $1.0 \times 10^{-4}$ m$^3$/min. The EMF value is measured by a Digital Multi Meter (Keithley 2001) with the input impedance of $10^9$ Ω.

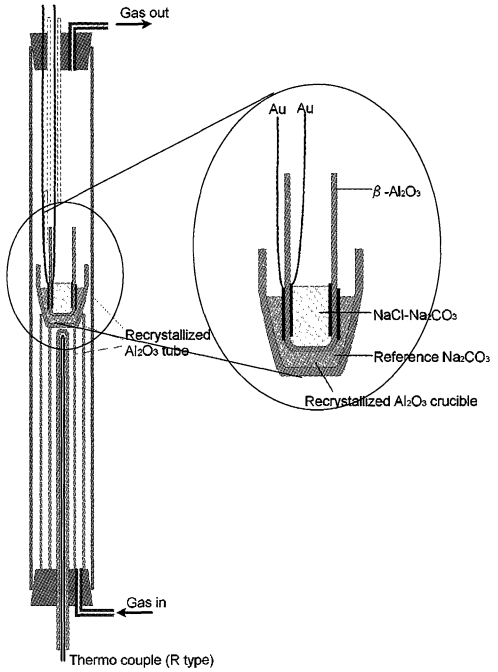


Fig. 2 Schematic illustration of Galvanic cell for the activity measurements of $Na_2CO_3$ in NaCl–$Na_2CO_3$ system.

## 3. Results and Discussion

### 3.1 Phase diagram for the NaCl–$Na_2CO_3$ system by the hot filament technique

The temperatures at which the sample states change were determined in both heating and cooling experiments. As the data obtained by cooling runs were 20°C lower than those by heating runs, the latter were adopted as the temperature of the phase change for the NaCl–$Na_2CO_3$ system, for the reason discussed in 3.2.

A typical result obtained in a heating run is shown in Fig. 3. The opaque sample, is initially a mixture of two solid phases of NaCl + $Na_2CO_3$ (Fig. 3(a)). At the eutectic temperature, the liquid phase is observed in the solid phase, and then two-phase coexistence (Fig. 3(b)) is observed above the eutectic temperature. The sample is then heated until the change from the solid + liquid phase to the complete single liquid phase (Fig. 3(c)) is observed to determine the liquidus tem-

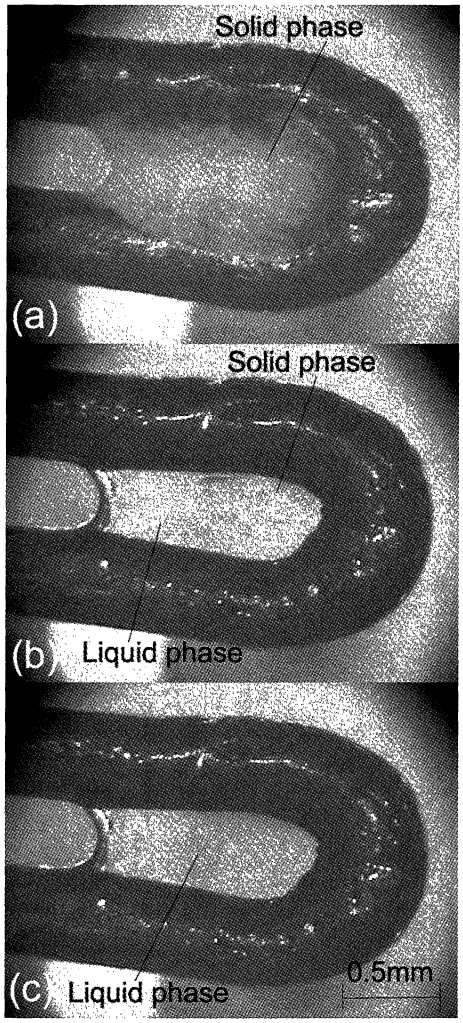


Fig. 3 Pictures of a sample on the hot filament; (a) a mixture of solid phases of NaCl+$Na_2CO_3$ at around 400°C, (b) a mixture of liquid+solid $Na_2CO_3$ above the eutectic temperature (about 700°C), and (c) a complete single liquid phase above the liquidus temperature (about 850°C).

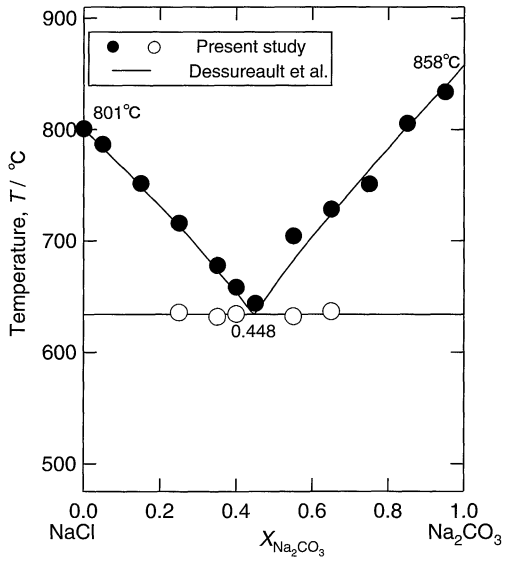


Fig. 4 Phase diagram for the NaCl–$Na_2CO_3$ system determined by the hot filament measurement on heating runs. Solid (●) and open circles (○) correspond to liquidus and eutectic temperatures, respectively.

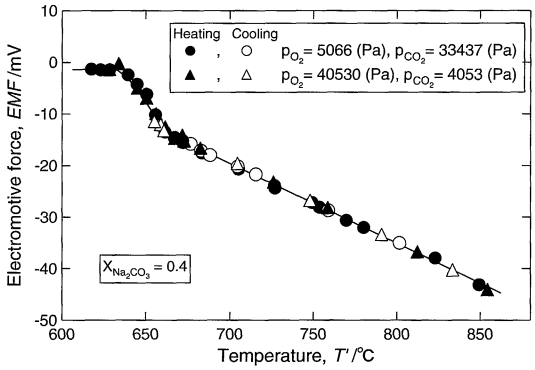


Fig. 5 EMF values measured for the composition of $X_{Na_2CO_3} = 0.4$ on cooling (open marks) and heating (solid marks) runs under different mixtures.

perature. The sample is finally gas-quenched for chemical analysis. The present results are summarized in the phase diagram in Fig. 4. Thirteen compositions were examined and the liquidus temperatures (indicated by solid circles in Fig. 4) are determined at respective compositions. For the samples with compositions close to the eutectic point, the estimated eutectic temperatures observed are shown by open circles in Fig. 4. The data measured in this study are very close to those reported earlier,[11] which are indicated by the solid lines.

### 3.2 $Na_2CO_3$ activities in the NaCl–$Na_2CO_3$ system

As typical results, EMF values measured for the sample $X_{Na_2CO_3} = 0.4$ are shown in Fig. 5. Data measured under the conditions of $p_{O_2} = 5066$(Pa), $p_{CO_2} = 33437$(Pa) and $p_{O_2} = 40530$(Pa), $p_{CO_2} = 4053$(Pa) are indicated by ●, ○ and ▲, △ respectively. EMF values are independent of the partial pressure of $O_2$ and $CO_2$, which is an indication of the attainment of equilibrium between gas phase and condensed phase. Data indicated by solid and open markers are EMF values measured on heating and cooling, respectively. The fact that these data also show good reproducibility between those measured by heating and cooling runs indicates that reversible EMFs were measured.

EMF values for the samples of $X_{Na_2CO_3} = 0.2$ and 0.4, in which the primary solid phase is NaCl are shown in Fig. 6. Knees of EMF curves are clearly observed at the temperatures where the phase relation changes. The phase diagram for the NaCl–$Na_2CO_3$ system is superimposed for comparison with the EMF-temperature diagram in Fig. 6. The EMF values stay at zero below the eutectic temperature because of the presence of pure solid $Na_2CO_3$. In the region above the eutectic temperature where the two-phase co-existence of liquid and pure solid NaCl is stable, the values of EMF begin to decrease sharply with temperature increase, and EMF values decrease with increasing temperature above the second knee corresponding to the liquidus point. EMF values of the NaCl–$Na_2CO_3$ mixture with compositions of $X_{Na_2CO_3} = 0.5$ and 0.7, where the primary solid phase is $Na_2CO_3$ are shown in Fig. 7. EMF values in the temperature region of both $Na_2CO_3$ + NaCl and $Na_2CO_3$ + liquid are zero due to the existence of pure solid $Na_2CO_3$. Above the liquidus temperature, where the single phase of liquid is stable, EMF values decreased with the increase in temperature.

$Na_2CO_3$ activities derived from EMF values using eq. (3)

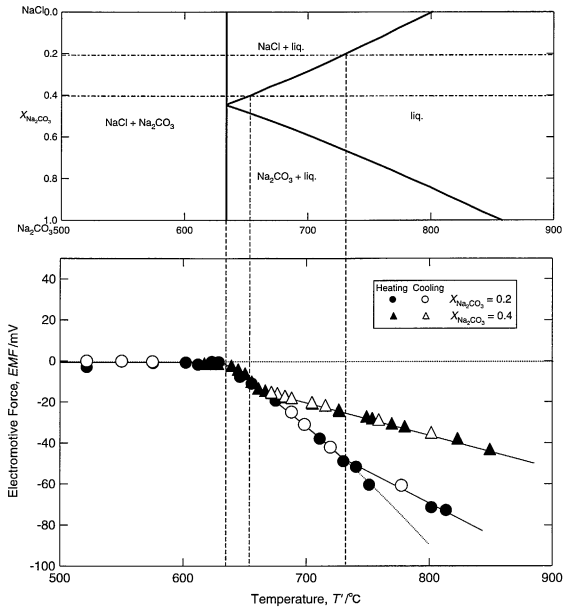


Fig. 6 EMF values measured for the composition of $X_{Na_2CO_3} = 0.2$ and 0.4. The upper figure indicates the phase diagram for the present system.

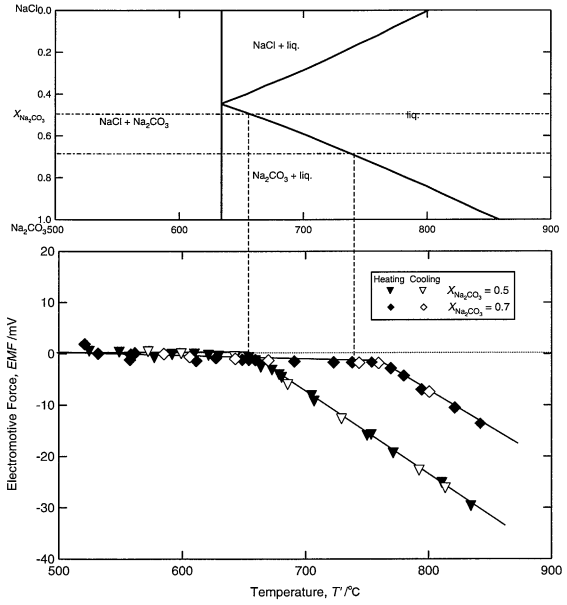


Fig. 7 EMF values measured for the composition of $X_{Na_2CO_3} = 0.5$ and 0.7. The upper figure indicates the phase diagram for the present system.

are shown in Fig. 8. Although several studies on the phase diagram for the NaCl–$Na_2CO_3$ system have been reported as mentioned in the previous section, there is no report available on the activity measurement of components in this system. Therefore, the present results are compared with those estimated from the parameter determined for the calculation of the phase diagram.[11] As the present system is a simple binary eutectic system without virtually any solid solubility for the terminal components, the thermodynamics parameters required to describe the system are limited to those for liquid phase. Dessureault *et al.* assessed the thermochemical properties of the present system[11] employing the equivalent fraction and the sub-regular model for liquid phase with Redlich-Kister type polynomial extension. The parameters for the liquid phase expressed as functions of a normal mole fraction, $X_{Na_2CO_3}$, as follows are very close to the ideal solution:

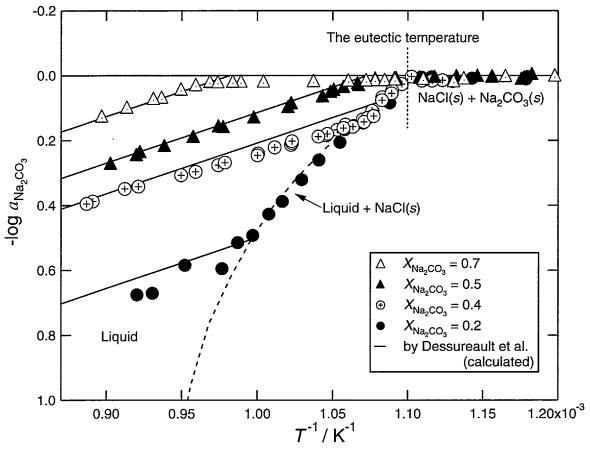


Fig. 8 Activity of $Na_2CO_3$ in the NaCl–$Na_2CO_3$ system as a function of reciprocal temperature. Solid lines and curve indicate the calculated activity based on the assessed thermodynamic data for liquid phase and liquidus line, respectively.

$$\Delta H^{ex,l}_{mix}/\mathrm{J{\cdot}mol^{-1}} = 996{\cdot}(1 - X_{Na_2CO_3}) \times X_{Na_2CO_3}/(1 + X_{Na_2CO_3}), \quad (4)$$

and

$$\Delta S^{ex,l}_{mix}/\mathrm{J{\cdot}K^{-1}{\cdot}mol^{-1}} = 0, \quad (5)$$

where $\Delta H^{ex,l}_{mix}$ and $\Delta S^{ex,l}_{mix}$ are the integral excess enthalpy and entropy change of mixing for the liquid phase. Employing these assessed parameters for the liquid phase, the values of EMF are calculated and shown by the solid lines in Fig. 8. Excellent agreement can be observed between experimental and calculated data, indicating the accurate assessment of the parameters due to the low degrees of arbitrariness in the assessment for the reasons below.

To further discuss the thermodynamic properties, the partial molar enthalpy ($\Delta \bar{H}^{ex,s}_{Na_2CO_3}$) and entropy ($\Delta \bar{S}^{ex,s}_{Na_2CO_3}$) changes of mixing for $Na_2CO_3$ relative to the pure solid $Na_2CO_3$ as the reference state are calculated by the least squares fitting of the relative chemical potential of $Na_2CO_3$ ($\Delta\mu_{Na_2CO_3} = RT \ln a^{solid}_{Na_2CO_3}$) to a simple linear equation by the Gibbs-Helmholtz equation; the results are plotted in Fig. 9. Values of both $\Delta \bar{H}^{ex,s}_{Na_2CO_3}$ and $\Delta \bar{S}^{ex,s}_{Na_2CO_3}$ show small variation with the composition. As the thermodynamic parameters given in eqs. (4) and (5) correspond to the thermodynamic quantities relative to pure liquid standard state for the terminal components, values of the standard enthalpy ($\Delta H^{fus}_{Na_2CO_3}$) and entropy ($\Delta S^{fus}_{Na_2CO_3}$) of fusion adopted in their calculation; $\Delta H^{fus}_{Na_2CO_3}/\mathrm{kJ{\cdot}mol^{-1}} = 29.665$ and $\Delta S^{fus}_{Na_2CO_3}/\mathrm{K^{-1}{\cdot}mol^{-1}} = 26.229$, respectively, should be added to $\Delta \bar{H}^{ex,l}_{Na_2CO_3}$ and $\Delta \bar{S}^{ex,l}_{Na_2CO_3}$ which were calculated from the assessed parameters, in order to estimate the values of $\Delta \bar{H}^{ex,s}_{Na_2CO_3}$ and $\Delta \bar{S}^{ex,s}_{Na_2CO_3}$ with pure solid $Na_2CO_3$ as the standard state. The calculated results are shown by solid curves in Fig. 9, indicating excellent agreement with the present ones. The experimental data are not sufficient and the scatters of the present results are relatively large, mak-

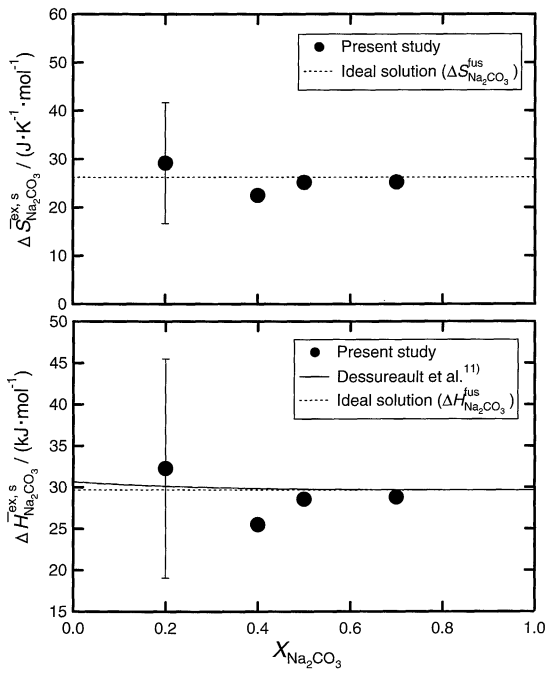


Fig. 9 Excess partial molar enthalpy ($\Delta \bar{H}^{ex,s}_{Na_2CO_3}$) and entropy ($\Delta \bar{S}^{ex,s}_{Na_2CO_3}$) of $Na_2CO_3$ obtained in this study and those calculated from assessed parameters by Dessureault *et al.*[11] The broken lines indicate the values of $\Delta H^{fus}_{Na_2CO_3}$ and $\Delta S^{fus}_{Na_2CO_3}$, which are added for the conversion of the standard state from the pure liquid state to the pure solid state.

ing it impossible to discuss the validity or accuracy of the reported parameters in detail. However, it is evident that the liquid phase can be primarily regarded as an ideal solution from the present results. This also confirms the phase diagram calculation because; when the ideal solution for liquid phase is assumed, the liquidus curves are almost the same as those reported the eutectic temperature and composition are 629°C and 0.446, which is very close to the values of 634°C and 0.448 calculated using the reported parameters.

### 3.3 Discussion of the metastability of NaCl–$Na_2CO_3$ melts

During the course of the present EMF measurements, positive values of EMF, corresponding to the $Na_2CO_3$ activity higher than unity were persistently and reproducibly observed below the eutectic temperature, when the cell was cooled faster than at 5°C/min. It should also be noted that no positive value is observed if the sample composition is in the region where the primary phase is $Na_2CO_3$. Figure 10 shows a typical example of temperature vs. $-\log a_{Na_2CO_3}$ plot for $X_{Na_2CO_3} = 0.2$, indicating the anomalous data marked X, Y, and Z by open squares (□) together with equilibrium values by open and closed circles. Taking into account the fact that no reliable data could be obtained from the hot filament measurements on decreasing temperature, one can suggest that attainment of the metastable state due to the supercooling of melts can be one possible explanation. This is caused by the suppression of $Na_2CO_3$ nucleation from melts in the eutectic reaction.

A quantitative analysis can be made using the free energy-composition diagram along with the cooling path as shown in Fig. 11. The Gibbs free energy change of the mixing for

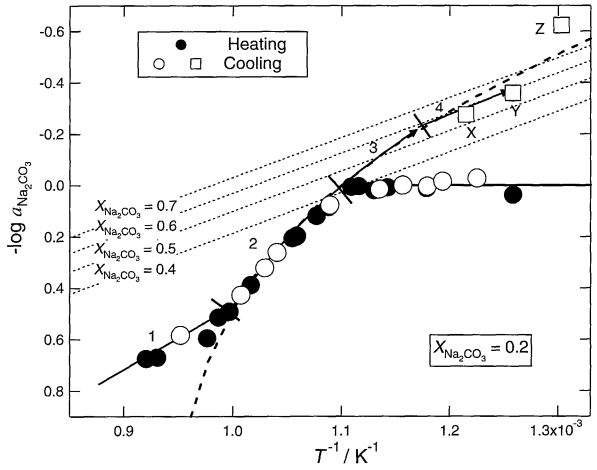


Fig. 10 Variation of measured EMF with temperature using the Galvanic cell constructed with $Na_2CO_3$ as a reference and $X_{Na_2CO_3} = 0.2$ as a sample. X, Y and Z indicate the anomalous EMFs. Thick lines indicate the equilibrium EMF. Thick broken curve indicates the equilibrium and metastable liquidus curve, and thin dotted lines correspond to the traces of the EMF for the respective compositions when the formation of all the solid phases is suppressed.

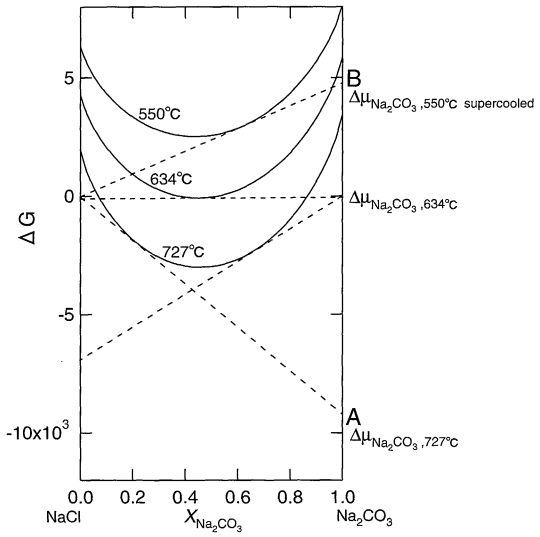


Fig. 11 Free energy-composition diagram for the NaCl–$Na_2CO_3$ system at 550, 634 and 727°C to explain the metastable cooling path.

the liquid phase, relative to pure solid $Na_2CO_3$ and NaCl, is estimated using thermodynamic parameters after Dessureault *et al.*[11] If an overall sample composition of $X_{Na_2CO_3} = 0.2$ is assumed, the sample is in the two-phase region of solid NaCl + liquid phase at 727°C. As the solid NaCl is already present as the primary solid phase, the growth of NaCl on NaCl precipitates proceeds as temperature decreases, and the composition of the liquid phase changes toward a lower NaCl direction. If the temperature reaches the eutectic temperature and if the nucleation of solid $Na_2CO_3$ is suppressed due to the large critical energy necessary for this solid nucleation, the melt will be supercooled with the metastable growth of NaCl. If the temperature reaches a certain point at which the diffusion of components necessary for the precipitation of $Na_2CO_3$ does not occur, the system is frozen in a metastable state. Subsequently, the supercooled melt may transform into a metastable glassy state after either stabilization or relax-

ation by the reduction of free volume. Such a supercooled state at 550°C is illustrated in Fig. 11 where all the extraneous effects of surface energy, stress, and stabilization by the change in the free volume are assumed to be negligible, and the free energy function of the liquid phase is simply employed for the calculation. As the solid NaCl and supercooled melt or glassy phase are in equilibrium at the interface, the common tangent law can be reasonably assumed. In this situation, the $Na_2CO_3$ activity is estimated as point B from the intersection of the common tangent line with the pure $Na_2CO_3$ axis, and the resultant activity of $Na_2CO_3$ is greater than unity. In this model, the composition of the supercooled melt changes to a value higher than the eutectic point, and is then quenched at a certain temperature and composition. The variation of $Na_2CO_3$ activity calculated from the model is plotted in Fig. 10, in which paths 1 through 4 correspond to the cooling paths in liquid (path 1), solid NaCl + liquid, (path 2), solid NaCl + supercooled liquid (path 3), and solid NaCl + quenched glassy state (path 4). Composition of the supercooled glassy state is estimated to be $X_{Na_2CO_3} = 0.574$ from this model. In case of the samples in the composition region where the primary solid phase is $Na_2CO_3$, the $Na_2CO_3$ activity is believed to remain at unity even when the supercooling occurs because of the presence of pure solid $Na_2CO_3$.

To examine the model mentioned above, variations of EMF during continuous cooling at the rates of 0.1, 0.5 and 1.0, where measured for $X_{Na_2CO_3} = 0.5$ and the results are shown in Fig. 12. At the liquidus and eutectic temperatures, anomalous changes in the slope of the plot are clearly observed. When the samples are cooled down from the uniform liquid phase, EMF values monotonously increase. When the temperature of the sample reaches at the eutectic temperature, no change in the EMF value is observed (see Fig. 12(b)) and the increase of EMF continues. Then, an abrupt EMF decrease is clearly observed. One of the possible explanations is given by the build-up of the supersaturation to gain the critical energy necessary for the nucleation of $Na_2CO_3$ from the liquid phase. The liquidus temperature corresponds to the intersection of extrapolated line of the two-phase region of solid $Na_2CO_3$ + liquid (termed as region 3 in Fig. 12(b)) and the trace of EMF in region 1, if the cooling condition is not far from equilibrium. The region 2 corresponds to the metastable liquid, which is formed by the critical energy for the nucleation of solid $Na_2CO_3$. It is not clear yet the reason why both the liquidus temperature estimated as mentioned above and the temperature at which the abrupt change occur, are almost independent of the cooling rate.

As for the eutectic reaction, multiple spikes observed at each cooling run correspond to the eutectic reactions. Shifts toward lower temperature with increase in the cooling rate are observed, similar to those observed common in differential thermal analysis (DTA). However, the variation of EMF values is too complicated to make further analysis possible. The authors suggest that the complex trace of EMF results from the large dimensions of the cell, which may cause an inhomogeneous temperature distribution. Further experiments are now underway using micro-cell apparatus, with the aim of developing a novel thermal analysis technique using the EMF method.

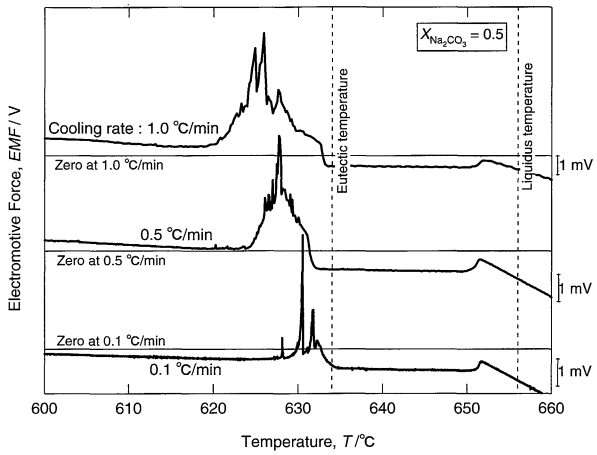


(a)

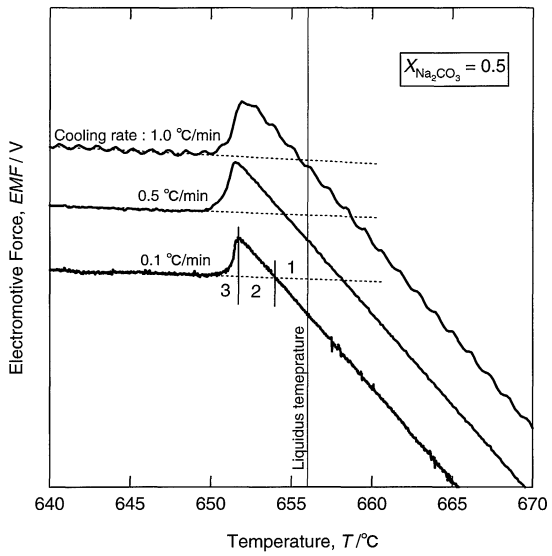


(b)

Fig. 12 (a) Continuous cooling curves of EMF at respective cooling rate for the sample of $X_{Na_2CO_3} = 0.5$. (b) Enlarged plots of the continuous cooling curves around liquidus temperature.

## 4. Conclusion

A phase diagram for the NaCl–$Na_2CO_3$ system has been determined from in-situ observation using a hot filament method. Liquidus and eutectic point are obtained in the present study. The eutectic temperature and composition is estimated as $X_{Na_2CO_3} = 0.43$ and 634°C, respectively, showing good agreement with those in earlier literature. Activities of $Na_2CO_3$ in the NaCl–$Na_2CO_3$ system have been determined by the EMF method using Na $\beta$-$Al_2O_3$ as a solid electrolyte. The present results show excellent agreement with activities calculated from thermodynamic data assessed by Dessureault *et al.*[11] from the phase diagram that the liquid phase is primarily regarded as an ideal solution. Also, formation of the metastable state at the eutectic reaction is suggested due to the suppression of solid $Na_2CO_3$ nucleation by the large critical energy. A new approach continuous cooling and heating measurements of EMF is examined to observe the detailed observation of the build-up of the metastable state as well as the development of a novel thermal analysis.

## Acknowledgements

The authors wish to express sincere thanks to Professor Toru H. Okabe of the Institute of Industrial Science, the University of Tokyo for his valuable discussions.

## REFERENCES

1) N. Nakashima, K. Hayashi, Y. Ohta, and K. Morinaga: Mater. Trans., JIM **32** (1991) 37–42.
2) M. Maeda and Y. Kariya: ISIJ Inter. **33** (1993) 182–187.
3) S. Ueda and M. Maeda: Metal. Mater. Trans. B **30B** (1999) 921–925.
4) K. Iwasawa and M. Maeda: Metal. Mater. Trans. B **31B** (2000) 795–799.
5) Y. F. Y. Yao and J. T. Kummer: J. Inorg. Nucl. Chem. **29** (1967) 2453–2475.
6) M. S. Whittingham and R. A. Huggins: J. Chem. Phys. **54** (1971) 414–416.
7) R. Galli, P. Longhi, T. Musshini and F. A. Tropeano: Electrochim. Acta **18** (1973) 1013–1016.
8) S. Yamaguchi, A. Imai, and K. S. Goto: J. Japan Inst. Metals **47** (1983) 736–742.
9) S. Yamaguchi and K. S. Goto: J. Japan Inst. of Metals **48** (1984) 779–786.
10) S. Yamaguchi, Y. Kaneko and Y. Iguchi: Trans. JIM **28** (1987) 986–993.
11) Y. Dessureault, J. Sangster and A. D. Pelton: Journal of Physical Chemistry Reference Data **19** No. 5 (1990) 1149–1178.